Molecular Vision 2015; 21:502-514 <http://www.molvis.org/molvis/v21/502>
Received 10 February 2015 | Accepted 27 April 2015 | Published 29 April 2015

Effect of HDAC Inhibitors on Corneal Keratocyte Mechanical Phenotypes in 3-D Collagen Matrices

Vindhya Koppaka, Neema Lakshman, W. Matthew Petroll

Department of Ophthalmology, University of Texas Southwestern Medical Center, Dallas, TX

Purpose: Histone deacetylase inhibitors (HDAC) have been shown to inhibit the TGFβ-induced myofibroblast transformation of corneal fibroblasts in 2-D culture. However, the effect of HDAC inhibitors on keratocyte spreading, contraction, and matrix remodeling in 3-D culture has not been directly assessed. The goal of this study was to investigate the effects of the HDAC inhibitors Trichostatin A (TSA) and Vorinostat (SAHA) on corneal keratocyte mechanical phenotypes in 3-D culture using defined serum-free culture conditions.

Methods: Rabbit corneal keratocytes were plated within standard rat tail type I collagen matrices (2.5 mg/ml) or compressed collagen matrices (~100 mg/ml) and cultured for up to 4 days in serum-free media, PDGF BB, TGFβ1, and either 50 nM TSA, 10 μM SAHA, or vehicle (DMSO). F-actin, α-SM-actin, and collagen fibrils were imaged using confocal microscopy. Cell morphology and global matrix contraction were quantified digitally. The expression of α-SM-actin was assessed using western blotting.

Results: Corneal keratocytes in 3-D matrices had a quiescent mechanical phenotype, as indicated by a dendritic morphology, a lack of stress fibers, and minimal cell-induced matrix remodeling. This phenotype was generally maintained following the addition of TSA or SAHA. TGFβ1 induced a contractile phenotype, as indicated by a loss of dendritic cell processes, the development of stress fibers, and significant matrix compaction. In contrast, cells cultured in TGFβ1 plus TSA or SAHA remained dendritic and did not form stress fibers or induce ECM compaction. Western blotting showed that the expression of α-SM actin after treatment with TGFβ1 was inhibited by TSA and SAHA. PDGF BB stimulated the elongation of keratocytes and the extension of dendritic processes within 3-D matrices without inducing stress fiber formation or collagen reorganization. This spreading response was maintained in the presence of TSA or SAHA.

Conclusions: Overall, HDAC inhibitors appear to mitigate the effects of TGFβ1 on the transformation of corneal keratocytes to a contractile, myofibroblast phenotype in both compliant and rigid 3-D matrices while preserving normal cell spreading and their ability to respond to the pro-migratory growth factor PDGF.

Because it is exposed, the cornea is susceptible to physical and chemical injuries, while also being a target of vision correction through refractive surgical procedures. Following a lacerating injury or refractive surgery, quiescent corneal keratocytes surrounding the wound often transform into fibroblasts or myofibroblasts, generating contractile forces and synthesizing scar tissue. These processes can cause a permanent reduction in corneal clarity, as well as decrease the effect of refractive surgery. TGFβ1, a cytokine key to modulating corneal wound healing, has been implicated in the development of corneal haze after photorefractive keratectomy (PRK) [1-4]. TGFβ1 has been shown to transform quiescent keratocytes into myofibroblasts that synthesize fibrotic extracellular matrix (ECM) and exert strong contractile forces [5-10]. These processes result in opacity and vision degradation in a subset of patients [11,12].

Correspondence to: W. Matthew Petroll, Department of Ophthalmology, Southwestern Medical Center, 5323 Harry Hines Blvd., Dallas, TX 75390-9057; Phone: (214) 648-7216; FAX: (214) 648-2382; email: matthew.petroll@utsouthwestern.edu

Histone deacetylase inhibitors (HDAC) have recently been shown to mitigate the effects of TGFβ1 both in vitro and in vivo. HDAC inhibitors were initially developed as anti-cancer agents for their ability to regulate epigenetically anti-angiogenic and pro-apoptotic gene expressions in transformed cells [13,14]. However, more recent studies have demonstrated their anti-inflammatory and anti-fibrotic properties in canine and equine corneal fibroblasts [15,16], as well as in animal models of inflammatory bowel disease, multiple sclerosis, and systemic lupus erythematosis [17]. A recent study showed the HDAC inhibitor Trichostatin A (TSA) could inhibit fibrosis during corneal wound healing in a rabbit PRK model [18]. Similarly, the topical application of Vorinostat (suberoylanilide hydroxamic acid [SAHA]), an FDA-approved analog of TSA, has been shown to significantly reduce corneal haze, the expression of the myofibroblast marker protein α-smooth muscle actin, and the inflammation associated with the wound healing response in the rabbit [19]. TSA and SAHA both belong to a structural class of hydroxamic acid-based inhibitors that are only effective against classes I, II, and IV HDACs containing zinc in their catalytic active site [20]. Recent studies have found that

inhibitors of these classes selectively alter the acetylation and transcription of genes involved in smooth muscle differentiation and fibrosis in cardiac fibroblasts [21,22]. However, their precise mechanism of action in reducing corneal fibrosis is still under investigation [23-25].

In vitro studies have shown that HDAC inhibitors can block myofibroblast transformation, but these studies have relied on 2-D culture models using serum-cultured corneal fibroblasts [18,23,24]. Keratocytes cultured under serum-free conditions maintain the quiescent, dendritic phenotype normally observed in vivo before injury [26,27], whereas exposure to serum results in fibroblast differentiation, as indicated by the assumption of a bipolar morphology, formation of intracellular stress fibers, and the downregulation of keratin sulfate proteoglycan expression [27-31]. An understanding of the effects of HDAC inhibition on both activated and quiescent corneal stromal cells is needed, as both are present during various stages of wound healing. The use of 3-D culture models may also provide further insights into the effect of HDAC inhibitors on cell behavior. Keratocytes reside within a complex 3-D extracellular matrix in vivo, and significant differences in cell morphology, adhesion organization, and mechanical behavior have been identified between 2-D and 3-D culture models [32-36]. Unlike rigid 2-D substrates, 3-D models also allow for the assessment of cellular force generation and cell-induced matrix reorganization, biomechanical activities that are critically involved in the migratory, contractile, and remodeling phases of wound healing. In this study, we use 3-D culture models to study the effects of HDAC inhibitors on TGFβ1-induced corneal keratocyte transformation (both biochemical and biomechanical) in defined serum-free culture conditions. We also evaluate the effects of these inhibitors on corneal keratocyte spreading in response to the pro-migratory growth factor PDGF [37,38].

METHODS

Cell culture: Corneal keratocytes were isolated from rabbit eyes obtained from Pel Freez (Rogers, AR) and cultured, as previously described [31]. Cells were cultured in flasks with a serum-free medium (basal medium) consisting of Dulbecco's modified Eagle's minimum essential medium with pyruvate (DMEM; Invtrogen, Carlsbad, CA) supplemented with 1% RPMI vitamin mix (Sigma-Aldrich, St. Louis, MO), 100 µM nonessential amino acids (Invitrogen), 100 µg/ml ascorbic acid, and 1% penicillin/streptomycin/amphotericin B (Lonza Walkersville, Inc., Walkersville, MD) to maintain the keratocyte phenotype [39].

Preparation of standard (uncompressed) collagen matrices: Hydrated collagen matrices were prepared by mixing Type I rat tail collagen (BD Biosciences, San Jose, CA) with 10X DMEM to achieve a final collagen concentration of 2.5 mg/ml [31]. A 50 ul of suspension of cells was added after neutralizing the collagen by addition of NaOH. Next, 30 ul aliquots of the cell/collagen mixture ($5x10^4$ cells/matrix) were spread over a central 12-mm diameter circular region on Bioptechs culture dishes (Delta T; Bioptechs, Inc., Butler, PA). The dishes were then placed in a humidified incubator for 30 min for polymerization. The matrices were overlaid with 1.5 ml of serum-free media (basal media). After 24 h of incubation to allow for cell spreading, the media were replaced with basal media, basal media supplemented with 50 ng/ml PDGF BB, or 10 ng/ml $TGF\beta_1$ and either 50 nM Trichostatin A (TSA; Sigma-Aldrich), 10 µM Vorinostat (suberoylanilidehydroxamic acid; SAHA; Selleck Chemicals LLC., Houston, TX), or vehicle (DMSO). Constructs were then cultured for an additional 1–4 days. Growth factor concentrations were determined from previous studies and they represent the lowest concentration to produce a maximal effect on changes in cell morphology and f-actin organization [37]. HDAC inhibitor concentrations were determined from pilot studies and they represent the highest concentration that did not induce keratocyte toxicity under serum-free conditions in standard 3-D collagen matrices.

Compressed collagen matrices: Compressed collagen matrices were prepared as described previously by Brown and coworkers [37,40,41]. Briefly, 10 mg/ml of Type I rat tail collagen (BD Biosciences) was diluted to a final concentration of 2 mg/ml. After drop-wise neutralization with 1M sodium hydroxide, a suspension of 2×10^4 or 2×10^5 keratocytes in 0.6 ml basal media was added to the collagen mixture. The solution containing cells and the collagen was poured into a 3×2×1 cm stainless steel mold and allowed to set for 30 min at 37 °C. To compact the matrices, a layer of nylon mesh (~50 µm mesh size) was placed on a double layer of filter paper. The matrices were placed on the nylon mesh, covered with a pane of glass, and loaded with a 130-g stainless steel block for 5 min at room temperature. This process squeezes media out of the matrix and results in the formation of a flat, cell/collagen sheet with high mechanical stiffness. Following compression, 6-mm diameter buttons were punched out of the matrix using a trephine [37]. After 24 h of incubation to allow for cell spreading, the media were replaced with basal media, basal media supplemented with 50ng/ml PDGF BB, or 10ng/ml $TGF\beta_1$ and either 50 nM TSA, 10 µM SAHA, or vehicle (DMSO). Constructs were then cultured for an additional 1–4 days.

Confocal imaging: After 1–4 days of culture in test media, cells were fixed using 3% paraformaldehyde in PBS for 15

min and permeabilized with 0.5% Triton X-100 in PBS for 3 min. To label f-actin, Alexa Fluor 546 phalloidin was used (1:20, Invitrogen). In some experiments, immunolabeling with α-smooth muscle actin (α-SM-actin) was performed. Following incubation in 1% BSA for 60 min to block non-specific binding, cells were incubated for 2 h in mouse monoclonal antibody α-SM-actin (1:100, Sigma Aldrich) in 1% BSA at 37 °C. Cells were then washed in PBS and incubated for 1 h in affinity-purified FITC conjugated goat anti-mouse IgG (1:20, Jackson Laboratories, Bar Harbor, ME). Nuclei were stained with DAPI (300 nM) for 5 min, washed, and placed in a ProLong® Gold anti-fade reagent for imaging.

Constructs were imaged using laser scanning confocal microscopy (Leica SP8, Heidelberg, Germany), as previously described [42]. A HeNe laser (633 nm) for reflection imaging, and Argon (488 nm) and GreNe (543 nm) lasers were used for fluorescent imaging. Stacks of optical sections (z-series) were acquired using a 63×water immersion objective (1.2 NA, 220 µm free working distance). Sequential scanning was used to image double-labeled samples to prevent cross-talk between fluorophores.

Cell morphology: Changes in cell morphology within compressed collagen matrices were measured using MetaMorph, as previously described [42]. The projected cell length was calculated by outlining the maximum intensity projection image of a cell (generated from the f-actin z-series), thresholding, and applying the Integrated Morphometry Analysis (IMA) routine. The length is calculated by IMA as the span of the longest chord through the object. The height of cells was calculated by measuring the distance between the first and last planes in the z-series in which a portion of the cell was visible. Measurements were performed on a minimum of 16 cells for each condition, taken from three separate experiments.

Global matrix contraction: DIC imaging was used to measure the global matrix contraction of standard (uncompressed) 3-D collagen matrices. As the bottoms of the matrices remain attached to the dish, cell-induced contraction results in a decrease in matrix height [43]. Height was measured by focusing on the top and bottom of each matrix at six different locations. Measurements were performed in triplicate for each condition and they were repeated 3X. The percentage decrease in the matrix height over time (as compared to control matrices without cells) was then calculated.

Immunoblotting: Hydrated collagen matrices with rabbit keratocytes were incubated in culture media with or without TGFβ1 (10 ng/ml), TSA (50 nM), and SAHA (10 uM) for 4 days. Post-incubation, cells were collected from the matrices (8–10 gels/precondition) through digestion in a solution of 2.5 mg/ml collagenase D (Roche Applied Sciences, IN) in PBS at 37 °C for 15 min, followed by centrifugation at 500 ×g for 4 min. Pelleted cells were washed in PBS and then lysed in ice-cold RIPA buffer (100 ul) supplemented with Protease, Phosphatase inhibitor cocktails (Roche Applied Sciences), PMSF (Sigma Aldrich), and sodium orthovandate (NEB) for 20 min. The lysates were sonicated on ice for 2 × 30 s at 30% power. Cell lysates were then clarified by centrifuging at 15,000 ×g at 4 °C for 45 min. The collected supernatant was assayed for total protein content using BCA assay (Thermo Scientific) and samples were prepared by adding 6X sample loading buffer (G Biosciences) with 20% β-mercaptoethanol and boiled for 5 min. An equal amount of protein (15 µg) from each condition was subjected to sodium dodecyl sulfate PAGE (SDS–PAGE) in 4–20% gels (Bio-Rad, Hercules, CA). The resolved proteins were then transferred onto a PVDF membrane (Millipore). The membrane was blocked with 5% non-fat milk in Tris buffered saline (TBS, pH 7.4) for 1 h at room temperature and incubated over night at 4 °C with mouse monoclonal anti-SMA antibody (1:1000; Sigma-Aldrich). The membrane was then washed in TBS-Tween-20 (0.1%) and probed with appropriate horseradish peroxidase (HRP)-conjugated secondary antibodies (1:10,000; Jackson laboratories) and enhanced chemiluminiscent (ECL) detection reagents (Pierce, Rockford, IL). Glyceraldehyde 3-phosphate dehydrogenase (GAPDH) was probed on each membrane to control for equal protein loading. The blots were imaged on a Typhoon Variable Mode Imager (Amersham Biosciences, NJ) and visualized using ImageJ Software.

Statistics: Statistical analyses were performed using SigmaStat version 3.11 (Systat Software Inc., Point Richmond, CA). A two-way repeated measures ANOVA was used to compare group means, and post-hoc multiple comparisons were performed using the Holm-Sidak method. Differences were considered significant if $p<0.05$.

RESULTS

Effect of TSA on corneal keratocyte phenotypes: Corneal keratocytes in standard (uncompressed) 3-D matrices had a quiescent mechanical phenotype, as indicated by a dendritic morphology, a lack of stress fibers, and minimal cell-induced matrix remodeling (Figure 1A). This phenotype was generally maintained following the addition of TSA (Figure 1B), although there was a reduction in the overall complexity and number of small branches in the cell processes. TGFβ1 induced a contractile phenotype, as indicated by a loss of dendritic cell processes, the development of stress fibers, and local matrix compaction (Figure 1C). In contrast, cells cultured in TGFβ1 plus TSA remained dendritic and did not

form stress fibers or induce ECM compaction (Figure 1D). A quantitative analysis of cell-induced ECM reorganization was assessed by measuring global matrix contraction (Figure 1E). An increase in global matrix contraction was induced by TGFβ1 at both 1 and 4 days of culture, and this increase was inhibited by TSA ($p<0.001$; two-way repeated measures ANOVA).

Consistent with previous studies, approximately 20% of cells showed positive labeling for α-SM-actin localized to the stress fibers following treatment with TGFβ1 in hydrated 3-D collagen matrices (Figure 2A). This was completely blocked by treatment with TSA (Figure 2B). TGFβ-treated cells also show enhanced vinculin labeling of focal contacts at the ends of stress fibers (Figure 2C), which was inhibited by TSA (Figure 2D). Western blotting showed the expression of α-SM actin after treatment with TGFβ1 for 4 days was inhibited by concurrent treatment with TSA (Figure 2E).

We also plated cells within compressed collagen matrices, as this provides a much stiffer 3-D culture environment than standard collagen matrices, similar to the native corneal stroma [40]. Specifically, the elastic modulus of newly polymerized 1–2 mg/ml hydrated collagen matrices measured by rheometry is generally less than 50 Pa [44-46], although the effective stiffness to which cells are exposed is likely higher in attached matrices due to the rigid boundary condition. By contrast, the stiffness of compressed collagen matrices has been reported to be 1 MPa [40,47] Keratocytes in compressed collagen matrices cultured in serum-free media developed a dendritic morphology with membrane-associated f-actin labeling (Figure 3A), as previously reported [37]. This cytoskeletal organization was maintained in the presence of TSA (Figure 3B). PDGF induces the branching and elongation of corneal keratocytes in 3-D matrices and is a potent stimulator of cell migration [37,38]. In this study, PDGF BB induced keratocyte spreading in compressed collagen matrices (Figure 3C), as indicated by an increase in the lengths of cells (Figure 3G). This spreading response was maintained in the presence of TSA (Figure 3D and G), although there was an apparent reduction in the number of branches and filopodial extensions along the dendritic processes. In contrast, TGFβ induced the loss of dendritic processes, stress fiber formation (Figure 3E), and the expression of α-SM-actin, as previously described [37]. This transformation was blocked by TSA (Figure 3F). Cells cultured in TGFβ were shorter and had a more stellate morphology than cells cultured in TGFβ + TSA (Figure 3G).

Effect of SAHA on corneal keratocyte phenotypes: Corneal keratocytes in hydrated 3-D collagen matrices also maintained their quiescent mechanical phenotype following the addition of SAHA (Figure 4A,B). Cells cultured in PDGF BB also maintained a quiescent mechanical phenotype and did not develop stress fibers or produce significant compaction of the matrix (Figure 4C). This response was maintained in the presence of SAHA (Figure 4D). Similar to TSA, SAHA prevented the TGFβ1-induced myofibroblast transformation of corneal keratocytes. Keratocytes cultured in TGFβ1 plus SAHA remained dendritic and did not form stress fibers or induce ECM compaction (compare Figure 4E,F). The expression of α-SM actin after treatment with TGFβ was also inhibited by SAHA (Figure 2E).

Similarly, in compressed collagen matrices, the normal dendritic morphology with membrane-associated f-actin labeling was maintained in the presence of SAHA (Figure 5A,B). PDGF BB induced keratocyte spreading in compressed collagen matrices, as indicated by an increase in the lengths of cells (Figure 5D). This spreading response was maintained in the presence of SAHA (Figure 5E). In both serum-free and PDGF culture conditions, there was an apparent reduction in the number of branches in the dendritic processes in the presence of SAHA. Similar to TSA, SAHA prevented the TGFβ1-induced myofibroblast transformation of corneal keratocytes inside compressed ECM (Figure 5C,D).

DISCUSSION

Corneal fibrosis following injury or surgery is characterized by the initial activation of keratocytes to a fibroblastic repair phenotype, some of which further differentiate into myofibroblasts. Myofibroblasts deposit excessive extracellular matrix components, generate large contractile forces, distort the surrounding microarchitecture, and ultimately contribute to corneal haze [2,6,7]. The HDAC inhibitors TSA and SAHA have demonstrated successful anti-inflammatory and anti-fibrogenic activity both in vitro and in vivo [48,49]. HDAC inhibition has been shown to reduce markedly laser-induced corneal haze in rabbits [18,19] and in alkali-burned mouse cornea in vivo [50]. In vitro studies have demonstrated HDAC inhibitors significantly decrease corneal fibroblast proliferation and activation and block TGFβ-induced alpha smooth muscle actin and fibrotic ECM expressions [15,16,23-25]. While these studies have provided important insights into the possible mechanism of the HDAC inhibition of corneal fibrosis, they used serum-cultured corneal fibroblasts plated on rigid 2-D substrates [18,23,24]; thus, the effect of HDAC inhibitors on keratocyte spreading, contraction, and matrix remodeling in 3-D culture has not been directly assessed. The goal of this study was to investigate the effects of the HDAC inhibitors TSA and SAHA on corneal keratocyte mechanical

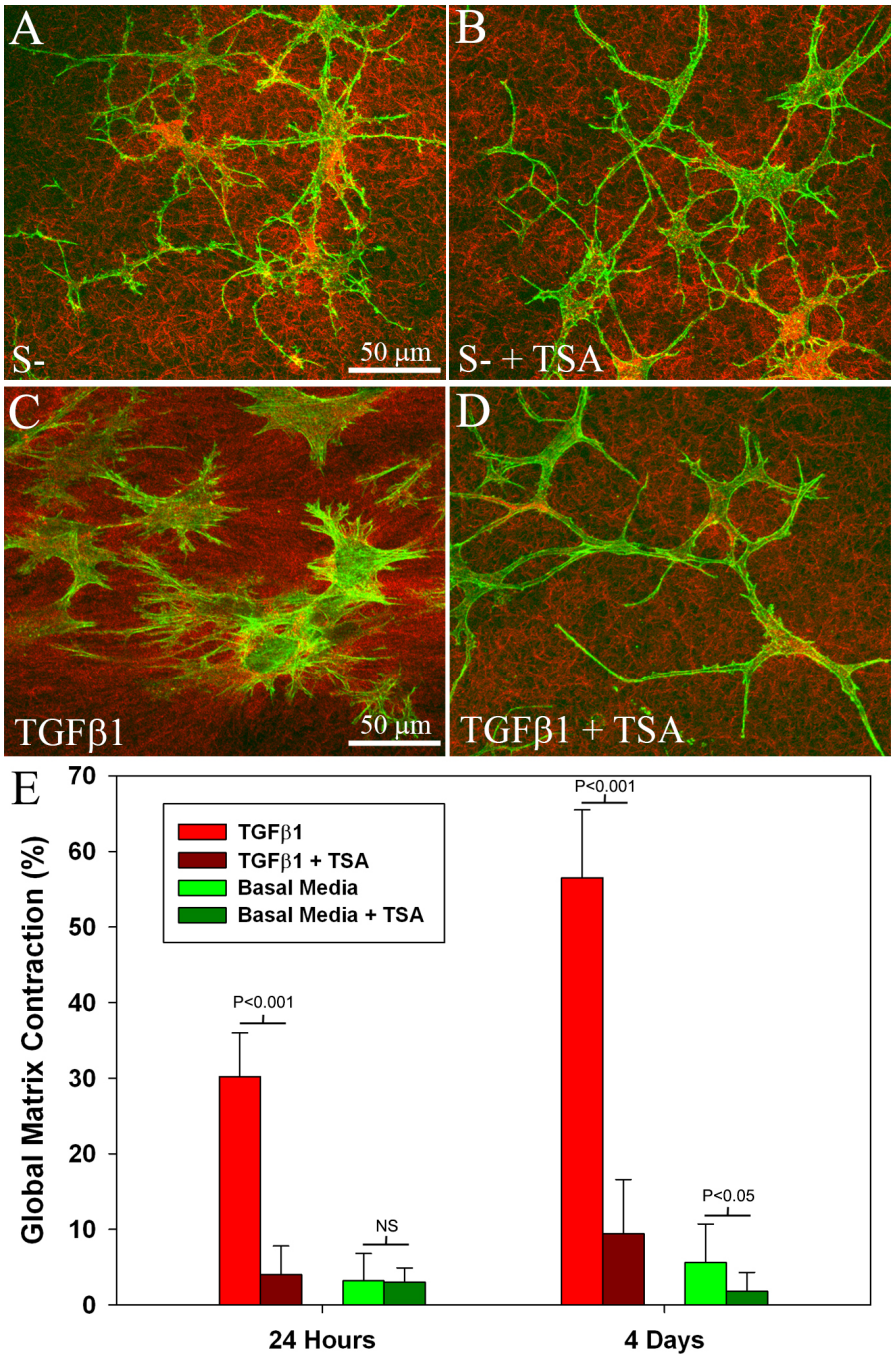

Figure 1. Effect of TSA on cell-induced matrix reorganization. **A-D**: Maximum intensity projection images of corneal keratocytes following 4 days of culture within 3-D collagen matrices. Green: f-actin; red: collagen. **A**: Keratocytes in basal serum-free media (S-) with vehicle have a dendritic morphology and a membrane-associated f-actin distribution, and they do not induce a significant compaction of collagen ECM. **B**: Keratocytes in basal media containing TSA have a similar phenotype. **C**: TGFβ1 induces a contractile phenotype, as indicated by a loss of dendritic cell processes, the development of stress fibers, and local matrix compaction. **D**: Cells cultured in TGFβ1 and TSA are elongated and do not form stress fibers or induce ECM compaction. **E**: A quantitative analysis of cell-induced ECM reorganization was assessed by measuring a global matrix contraction. An increase in global matrix contraction was induced by TGFβ1 at both 1 and 4 days of culture, and this increase was inhibited by TSA ($p<0.001$; two-way repeated measures ANOVA). Measurements were performed in triplicate for each condition, and repeated 3 times.

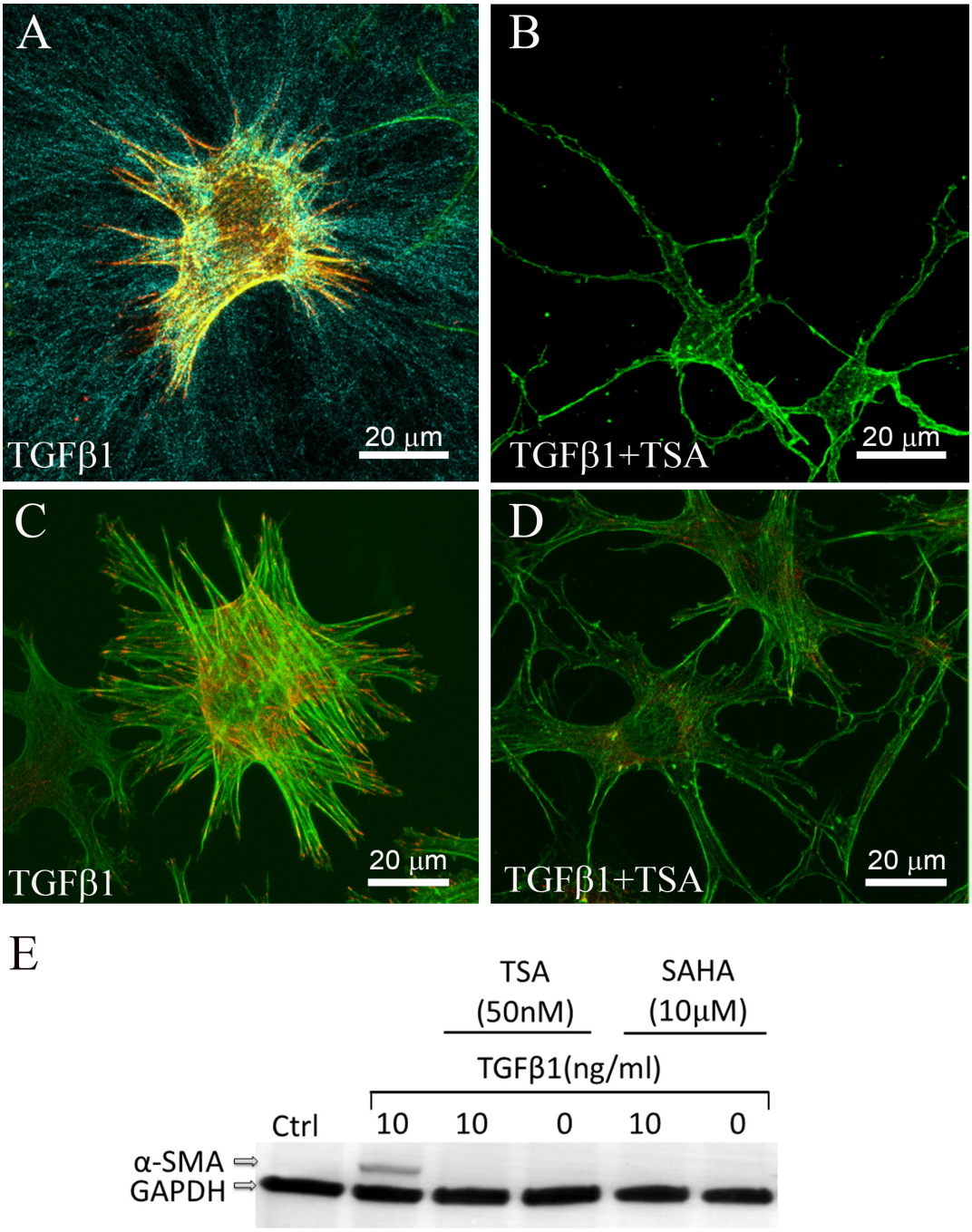

Figure 2. Effect of TSA on TGFβ-induced myofibroblast transformation. **A**: In hydrated 3-D collagen matrices, approximately 20% of cells show positive labeling for α-SM-actin localized to the stress fibers following 4 days of treatment with TGFβ1. Green: f-actin; red: α-SM-actin; cyan: collagen. **B**: Labeling for α-SM-actin was not observed following treatment with TSA. Green: f-actin; red: α-SM-actin. **C**: TGFβ1-treated cells also show enhanced vinculin labeling of focal contacts at the ends of stress fibers, which was inhibited by TSA (**D**). Green: f-actin; red: vinculin. **E**: western blot analysis from cell extracts showing the expression of α-SM actin after treatment with TGFβ1, TGFβ1 + TSA, or TGFβ1 + SAHA. TSA and SAHA both inhibited the expression of α-SM actin. The result is representative of two independent experiments.

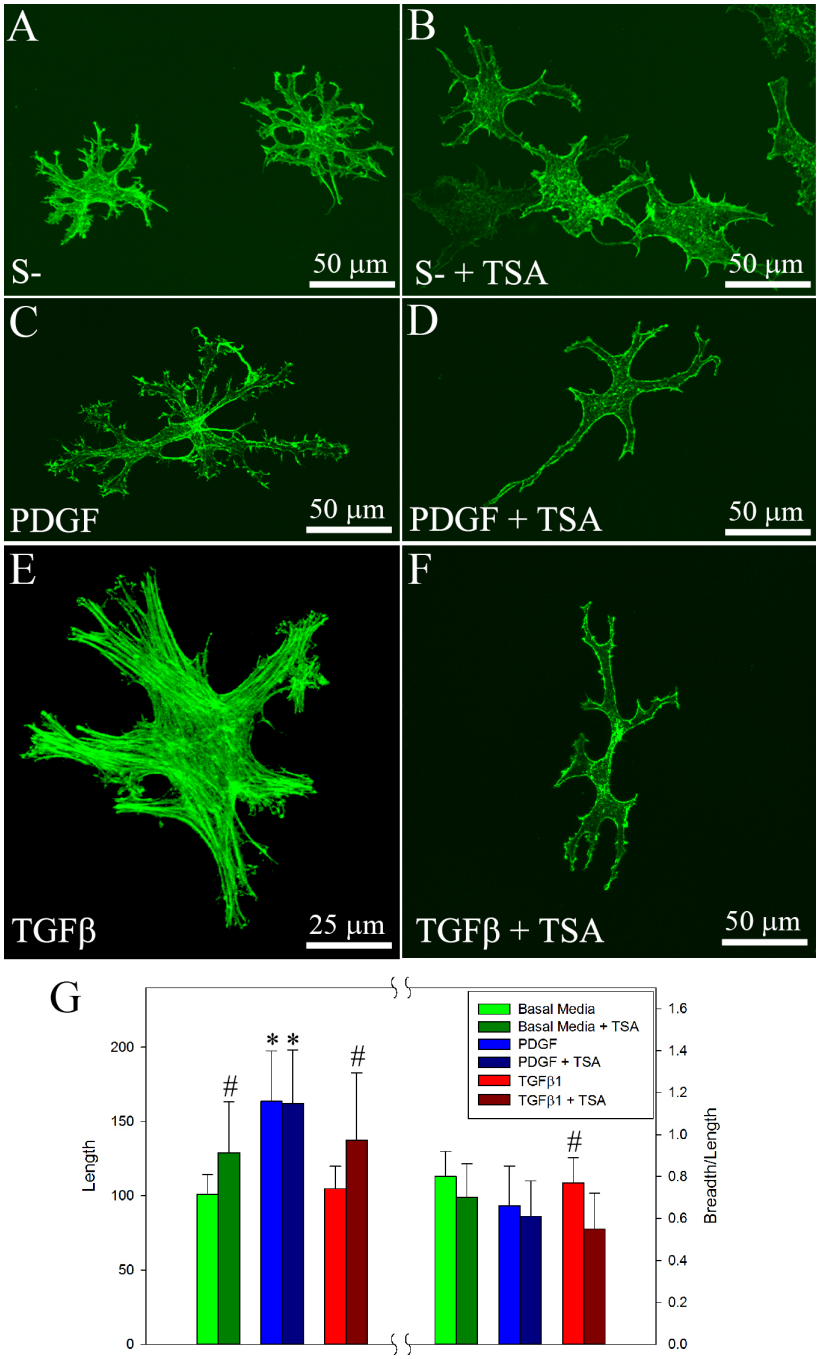

Figure 3. Effect of TSA on keratocyte phenotypes in compressed collagen matrices. Maximum intensity projection images of f-actin organization in corneal keratocytes following 4 days of culture within compressed collagen matrices. **A**: Keratocytes in compressed collagen matrices cultured in basal serum-free media (S-) with vehicle developed a dendritic morphology with membrane-associated f-actin labeling, and this morphology was maintained in the presence of TSA (**B**). **C**: PDGF BB induced keratocyte spreading in compressed collagen matrices without inducing stress fiber formation, and this spreading response was maintained in the presence of TSA (**D**). **E**: TGFβ1 induced the loss of dendritic processes and the formation of stress fibers, and this transformation was blocked by TSA (**F**). **G**: Left side of graph shows cell length following 4 days of culture inside compressed ECM. *PDGF induced a significant increase in cell length as compared to basal media and TGFβ, both with and without TSA ($p<0.05$, two way ANOVA). #In both basal media and TGF1β, cell length was greater in the presence of TSA ($p<0.05$, two way ANOVA). Right side of graph shows breadth/length following 4 days of culture. #Cells cultured in TGFβ1 were less elongated than cells cultured in TGFβ1 + TSA ($p<0.05$, two way ANOVA). Measurements were performed on a minimum of 16 cells for each condition, taken from three separate experiments.

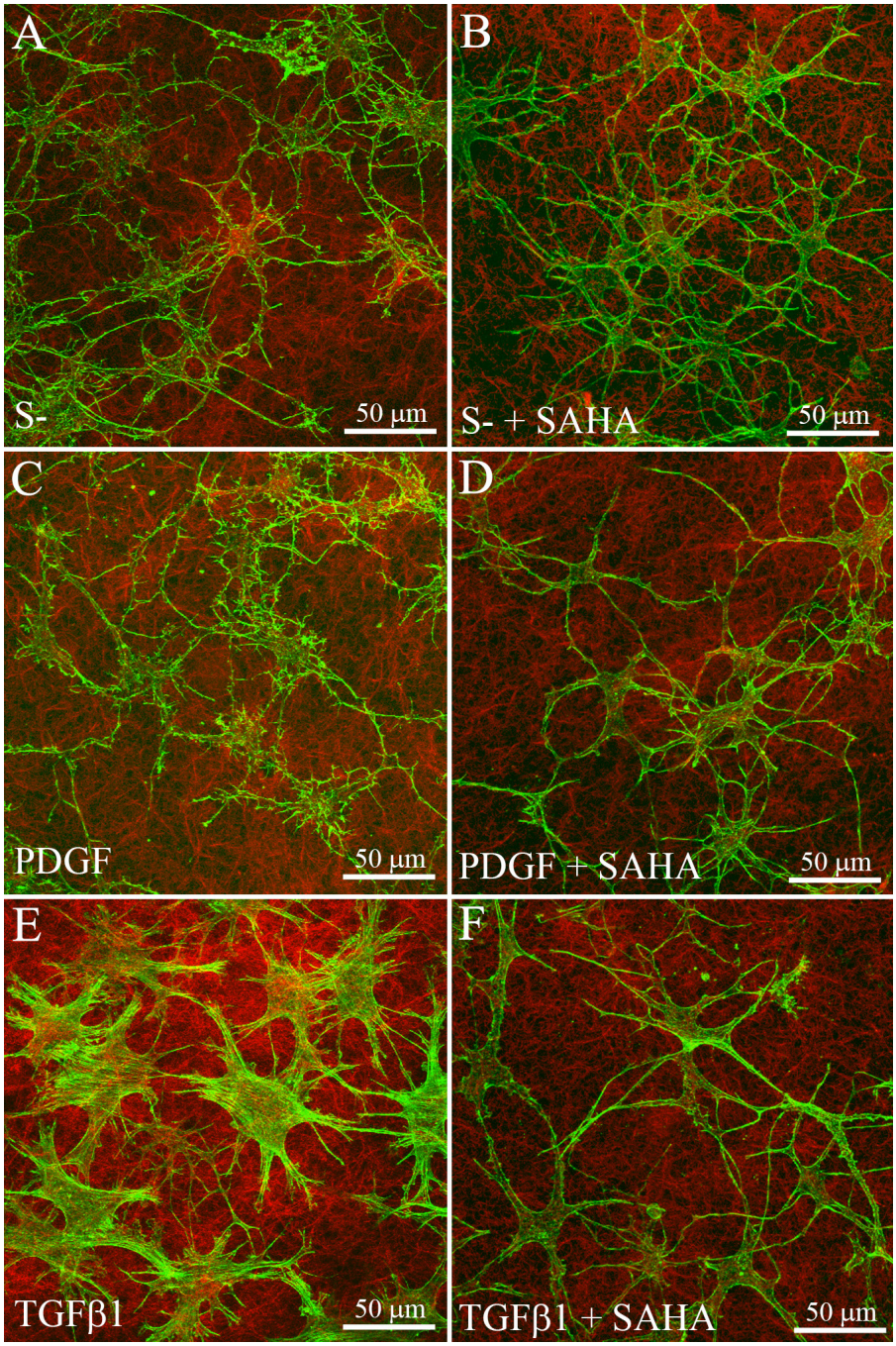

Figure 4. Effect of SAHA on cell-induced matrix reorganization. **A-F**: Maximum intensity projection images of corneal keratocytes following 4 days of culture within 3-D collagen matrices. Green: f-actin; red: collagen. **A**: Keratocytes in basal serum-free media (S-) with vehicle have a dendritic morphology and a membrane-associated f-actin distribution, and they do not induce a significant compaction of collagen ECM. **B**: Keratocytes in basal media containing SAHA have a similar phenotype. **C**: PDGF BB induced the formation and elongation of dendritic cell processes without inducing stress fiber formation, and this spreading response was maintained in the presence of SAHA (**D**). **E**: TGFβ1 induces a contractile phenotype, as indicated by a loss of dendritic cell processes, the development of stress fibers, and local matrix compaction. **F**: Cells cultured in TGFβ1 plus SAHA are elongated and do not form stress fibers or induce ECM compaction.

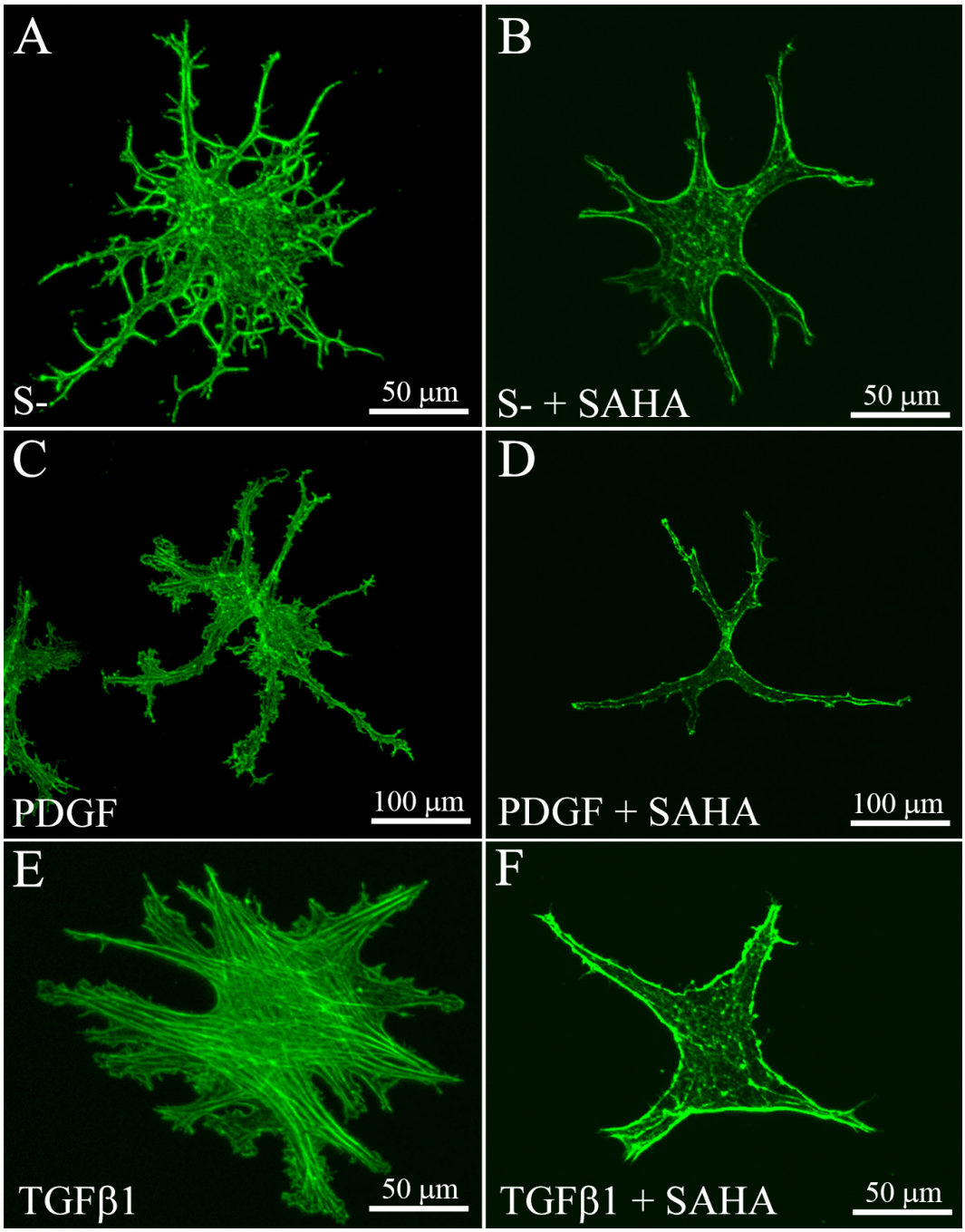

Figure 5. Effect of SAHA on keratocyte phenotypes in compressed collagen matrices. Maximum intensity projection images of f-actin organization in corneal keratocytes following 4 days of culture within compressed collagen matrices. **A**: Keratocytes in compressed collagen matrices cultured in basal serum-free media (S-) with vehicle developed a dendritic morphology with membrane-associated f-actin labeling, and this morphology was maintained in the presence of SAHA (**B**). **C**: PDGF BB induced keratocyte spreading in compressed collagen matrices without inducing stress fiber formation, and this spreading response was maintained in the presence of SAHA (**D**). **E**: TGFβ1 induced the loss of dendritic processes and the formation of stress fibers, and this transformation was blocked by SAHA (**F**).

phenotypes in 3-D culture using defined serum-free culture conditions.

We show for the first time that TGFβ1-induced morphological changes, stress fiber formation, and matrix reorganization in corneal keratocytes in 3-D collagen matrices were inhibited by both TSA and SAHA. Concurrently, the expression of alpha-SMA was blocked by these HDAC inhibitors. Mechanistically, the HDAC inhibitors may lead to increased histone acetylation, thereby decreasing transcriptional access to gene promoter regions of pro-fibrotic proteins, such as α-SMA. The TGFβ-induced reorganization of the actin cytoskeleton and enhanced contractility have been shown to be products of increased transcription and the activation of small GTPases and RhoA/B, which themselves have been shown to be activated by TGFβ-dependent Smad proteins in NIH3T3 fibroblasts [51]. In addition, Smad3 mediates the TGFβ-induced α-SMA expression in rat lung fibroblasts [52]. Interestingly, the upregulation of α-SMA in corneal myofibroblasts stimulated by TGFβ is attenuated by inhibiting Rho-associated protein kinase (ROCK), a downstream target of Rho GTPase signaling that regulates cell contractility [37,53]. This suggests a possible interplay between the Rho signaling pathway and Smad proteins in TGFβ-induced fibrosis, both of which may likely be influenced by HDAC activity.

In addition to TGFβ, another growth factor that may play an important role in wound healing is PDGF, which is endogenously expressed in corneal tear fluid and has been shown to induce cell spreading and migration in both dermal and corneal fibroblasts [38,43,54]. Specifically, PDGF BB induces Rac activation, which results in cell spreading via the formation of extensive pseudopodial processes and membrane ruffling with increased cell length and area in 3-D matrices [54]. PDGF stimulates the migration of corneal keratocytes without the generation of large mechanical forces, as indicated by a lack of stress fibers and minimal cell-induced ECM reorganization [37]. Thus, PDGF may facilitate wound repopulation without the development of fibrotic tissue, which can impair vision. In this study, corneal keratocytes elongated when stimulated with PDGF BB, even in the presence of TSA or SAHA, suggesting PDGF-induced cell spreading and migration may persist despite a loss in HDAC activity. Cells also maintained a quiescent mechanical phenotype in PDGF BB, as indicated by the maintenance of dendritic cell processes, a lack of stress fibers, and minimal cell-induced matrix reorganization. One difference we observed in the keratocyte phenotype following HDAC inhibition in both serum-free and PGDF containing media was a reduction in the branching and short filopodial extensions along the dendritic cell processes. The significance of this finding is unclear.

Studies using other cell types have shown that deacetylase activity may be required for PDGF-induced actin remodeling and cell migration [55]. In NIH3T3 fibroblasts, deacetylase activity is required for certain PDGF-induced transcriptional programs, particularly STAT3 activation [56] and its dependent transcription of growth stimulatory genes (c-myc) [57], the induction of anti-apoptotic (bcl-XL) [58], and pro-angiogenetic (VEGF) activities [59]. Others have found HDAC6 (a potent class II microtubule deacetylase [55]) activity to be necessary [60,61] but not sufficient to support cell migration through the deacetylation of alpha-tubulin [62]. This may be explained by the fact that in addition to microtubules [61], deacetylase activity also targets the function of the molecular chaperone heat shock protein 90 (Hsp90) [63,64], a requirement for PDGF-induced membrane ruffle formation and cell motility. The expression of an acetylation-resistant mutant form of Hsp90 in HDAC6-deficient mouse embryonic fibroblasts rescued membrane ruffle defects in these cells [62]. Finally, functional HDAC6 and Hsp90 activity together were shown to be important for a fully activated Rac1 and consequent cell migration [62]. However, we also note that HDAC6-deficient mice are viable and fertile and show no obvious defects in microtubule organization and stability, despite impaired Hsp90 function [65]. Thus, there may be redundant mechanisms controlling actin organization and cell migration in these mice, which may explain the persistent spreading of corneal keratocytes after PDGF treatment, despite the inhibition of HDAC6 activity by TSA and SAHA in this study.

The similarity in the effects of TSA and SAHA were as expected, as both inhibitors are analogs targeting the same class I and II HDACs, which require zinc for their catalytic activity. Inhibitors such as TSA and SAHA show low selectivity for the individual isoforms of class I and II HDACs, furthering the need to develop novel isozyme-specific inhibitors. This will be an important step toward addressing the dearth of knowledge regarding discovering and validating functional targets of each of these HDAC enzymes, in addition to identifying differences between their catalytic and non-catalytic activities.

Overall, the data demonstrate that HDAC inhibitors mitigate the effects of TGFβ1 in the transformation of quiescent corneal keratocytes to a contractile, myofibroblast phenotype in both compliant and rigid 3-D matrices, while preserving normal cell spreading and their ability to respond to the pro-migratory growth factor PDGF BB. Following corneal injury, quiescent keratocytes are still present in the

stroma surrounding the wound. From a clinical standpoint, it is important that HDAC inhibitors block TGFβ-induced myofibroblast transformation and its associated fibrosis, but that they do not alter the normal phenotype of these cells. In addition, the ability of keratocytes to respond to other wound healing cytokines, such as PDGF, following HDAC inhibition may allow keratocytes to repopulate the wounded stroma while maintaining a more quiescent cell mechanical phenotype and a more regenerative wound healing process.

ACKNOWLEDGMENTS

This study was supported in part by NIH R01EY013322, NIH P30EY020799, and an unrestricted grant from Research to Prevent Blindness, Inc., NY. We would also like to acknowledge Devansh Trivedi for his participation in pilot experiments, preceding the execution of this study.

REFERENCES

1. Møller-Pedersen T, Cavanagh HD, Petroll WM, Jester JV. Neutralizing antibody to TGFβ modulates stromal fibrosis but not regression of photoablative effect following PRK. Curr Eye Res 1998; 17:736-7. [PMID: 9678420].
2. Jester JV, Petroll WM, Cavanagh HD. Corneal stromal wound healing in refractive surgery: the role of the myofibroblast. Prog Retin Eye Res 1999; 18:311-56. [PMID: 10192516].
3. Jester JV, Barry-Lane PA, Petroll WM, Olsen DR, Cavanagh HD. Inhibition of cornea fibrosis by topical application of blocking antibodies to TGFβ in the rabbit. Cornea 1999; 16:177-87. .
4. Chen C, Michelini–Norris B, Stevens S, Rowsey J, Ren X-o, Goldstein M, Schultz G. Measurement of mRNAs for TGFβ and extracellular matrix proteins in corneas of rats after PRK. Invest Ophthalmol Vis Sci 2000; 41:4108-16. [PMID: 11095603].
5. Jester JV, Barry-Lane PA, Cavanagh HD, Petroll WM. Induction of alpha-smooth muscle actin expression and myofibroblast transformation in cultured corneal keratocytes. Cornea 1996; 15:505-16. [PMID: 8862928].
6. Hinz B. The myofibroblast: Paradigm for a mechanically active cell. J Biomech 2010; 43:146-55. [PMID: 19800625].
7. Wilson SE. Corneal myofibroblast biology and pathobiology: generation, persistence, and transparency. Exp Eye Res 2012; 99:78-88. [PMID: 22542905].
8. Jester JV, Huang J, Barry-Lane PA, Kao WW, Petroll WM, Cavanagh HD. Transforming growth factor(beta)-mediated corneal myofibroblast differentiation requires actin and fibronectin assembly. Invest Ophthalmol Vis Sci 1999; 40:1959-67. [PMID: 10440249].
9. Jester JV, Huang J, Fisher S, Spiekerman J, Chang JH, Wright WE, Shay JW. Myofibroblast differentiation of normal human keratocytes and hTERT, extended-life, human corneal fibroblasts. Invest Ophthalmol Vis Sci 2003; 44:1850-8. [PMID: 12714615].
10. Jester JV, Huang J, Petroll WM, Cavanagh HD. TGFbeta induced myofibroblast differentiation of rabbit keratocytes requires synergistic TGFbeta, PDGF and integrin signalling. Exp Eye Res 2002; 75:645-57. [PMID: 12470966].
11. Moller-Pedersen T, Cavanagh HD, Petroll WM, Jester JV. Stromal wound healing explains refractive instability and haze development after photorefractive keratectomy: A 1-year confocal microscopic study. Ophthalmology 2000; 107:1235-45. [PMID: 10889092].
12. Dupps WJ, Wilson SE. Biomechanics and wound healing in the cornea. Exp Eye Res 2006; 83:709-20. [PMID: 16720023].
13. Bolden JE, Peart MJ, Johnstone RW. Anticancer activities of histone deacetylase inhibitors. Nat Rev Drug Discov 2006; 5:769-84. [PMID: 16955068].
14. West AC, Johnstone RW. New and emerging HDAC inhibitors for cancer treatment. J Clin Invest 2014; 124:30-9. [PMID: 24382387].
15. Bosiack AP, Giuliano EA, Gupta R, Mohan RR. Efficacy and safety of suberoylanilide hydroxamic acid (Vorinostat) in the treatment of canine corneal fibrosis. Vet Ophthalmol 2012; 15:307-14. [PMID: 22212187].
16. Donnelly KS, Giuliano EA, Sharm A, Mohan RR. Suberoylanilide hydroxamic acid (vorinostat): its role on equine corneal fibrosis and matrix metalloproteinase activity. Vet Ophthalmol 2014; 17:Suppl 161-8. [PMID: 25126665].
17. Adcock IM. HDAC inhibitors as anti-inflammatory agents. Br J Pharmacol 2007; 150:829-31. [PMID: 17325655].
18. Sharma A, Mehan MM, Sinha S, Cowden JW, Mohan RR, Trichostatin A. Trichostatin A inhibits corneal haze in vitro and in vivo. Invest Ophthalmol Vis Sci 2009; 50:2695-701. [PMID: 19168895].
19. Tandon A, Tovey JC, Waggoner MR, Sharma A, Cowden JW, Gibson DJ, Liu Y, Schultz GS, Mohan RR. Vorinostat: a potent agent to prevent and treat laser-induced corneal haze. J Refract Surg 2012; 28:285-90. [PMID: 22386369].
20. Vannini A, Volpari C, Filocamo G, Casavola EC, Brunetti M, Renzoni D, Chakravarty P, Paolini C, De Francesco R, Gallinari P, Steinkühler C, Di Marco S. Crystal structure of a eukaryotic zinc-dependent histone deacetylase, human HDAC8, complexed with a hydroxamic acid inhibitor. Proc Natl Acad Sci USA 2004; 101:15064-9. [PMID: 15477595].
21. Tang Y, Boucher JM, Liaw L. Histone deacetylase activity selectively regulates notch-mediated smooth muscle differentiation in human vascular cells. J Am Heart Assoc 2012; 1:e000901-[PMID: 23130137].
22. Nural-Guvener HF, Zakharova L, Nimlos J, Popovic S, Mastroeni D, Gaballa MA. HDAC class I inhibitor, Mocetinostat, reverses cardiac fibrosis in heart failure and diminishes CD90+ cardiac myofibroblast activation. Fibrogenesis Tissue Repair 2014; 7:10-[PMID: 25024745].
23. Yang L, Qu M, Wang Y, Duan H, Chen P, Wang Y, Shi W, Danielson P, Zhou Q. Trichostatin A inhibits transforming

growth factor-beta-induced reactive oxygen species accumulation and myofibroblast differentiation via enhanced NF-E2-related factor 2-antioxidant response element signaling. Mol Pharmacol 2013; 83:671-80. [PMID: 23284002].

24. Zhou Q, Yang L, Wang Y, Qu M, Chen P, Wang Y, Xie L, Zhao J, Wang Y. TGFbeta mediated transition of corneal fibroblasts from a proinflammatory state to a profibrotic state through modulation of histone acetylation. J Cell Physiol 2010; 224:135-43. [PMID: 20232294].

25. Zhou Q, Wang Y, Yang L, Wang Y, Chen P, Wang Y, Dong X, Xie L. Histone deacetylase inhibitors blocked activation and caused senescence of corneal stromal cells. Mol Vis 2008; 14:2556-65. [PMID: 19122829].

26. Beales MP, Funderburgh JL, Jester JV, Hassell JR. Proteoglycan synthesis by bovine keratocytes and corneal fibroblasts: maintenance of the keratocyte phenotype in culture. Invest Ophthalmol Vis Sci 1999; 81658-63. [PMID: 10393032].

27. Jester JV, Barry PA, Lind GJ, Petroll WM, Garana R, Cavanagh HD. Corneal keratocytes: In situ and in vitro organization of cytoskeletal contractile proteins. Invest Ophthalmol Vis Sci 1994; 35:730-43. [PMID: 8113024].

28. Dahl IMS. Biosynthesis of proteoglycans and hylauronate in rabbit corneal fibroblast cultures: variation with age of the cell line and effect of fetal calf serum. Exp Eye Res 1981; 32:419-33. [PMID: 7238627].

29. Hassell JR, Schrecengost PK, Rada JA, Sundaraj N, Sosi G, Thot RA. Biosynthesis of stromal matrix proteoglycans and basement membrane components by human corneal fibroblasts. Invest Ophthalmol Vis Sci 1992; 33:547-57. [PMID: 1544783].

30. Funderburgh JL, Mann MM, Funderburgh ML. Keratocyte phenotype mediates proteoglycan structure: a role for fibroblasts in corneal fibrosis. J Biol Chem 2003; 278:45629-37. [PMID: 12933807].

31. Lakshman N, Kim A, Petroll WM. Characterization of corneal keratocyte morphology and mechanical activity within 3-D collagen matrices. Exp Eye Res 2010; 90:350-9. [PMID: 20025872].

32. Tomasek JJ, Hay ED, Fujiwara K. Collagen modulates cell shape and cytoskeleton of embryonic corneal and fibroma fibroblasts: Distribution of actin, α-actinin and myosin. Dev Biol 1982; 92:107-22. [PMID: 7106372].

33. Cukierman E, Pankov R, Yamada KM. Cell interactions with three-dimensional matrices. Curr Opin Cell Biol 2002; 14:633-9. [PMID: 12231360].

34. Grinnell F, Petroll WM. Cell motility and mechanics in three-dimensional collagen matrices. Annu Rev Cell Dev Biol 2010; 26:335-61. [PMID: 19575667].

35. Bard JBL, Hay ED. The behavior of fibroblasts from the developing avian cornea: Morphology and movement in situ and in vitro. J Cell Biol 1975; 67:400-18. [PMID: 1194354].

36. Doane KJ, Birk DE. Fibroblasts retain their tissue phenotype when grown in three-dimensional collagen gels. Exp Cell Res 1991; 195:432-42. [PMID: 2070825].

37. Kim A, Lakshman N, Karamichos D, Petroll WM. Growth factor regulation of corneal keratocyte differentiation and migration in compressed collagen matrices. Invest Ophthalmol Vis Sci 2010; 51:864-75. [PMID: 19815729].

38. Kim A, Zhou C, Lakshman N, Petroll WM. Corneal stromal cells use both high- and low-contractility migration mechanisms in 3-D collagen matrices. Exp Cell Res 2012; 318:741-52. [PMID: 22233682].

39. Jester JV, Chang J-H. Modulation of cultured corneal keratocyte phenotype by growth factors/cytokines control in vitro contractility and extracellular matrix contraction. Exp Eye Res 2003; 77:581-92. [PMID: 14550400].

40. Brown RA, Wiseman M, Chuo C-B, Cheema U, Nazhat SN. Ultrarapid engineering of biomimetic materials and tissues: fabrication of nano- and microstructures by plastic compression. Adv Funct Mater 2005; 15:1762-70. .

41. Neel EAA, Cheema U, Knowles JC, Brown RA, Nazhat SN. Use of multiple unconfined compression for control of collagen gel scaffold density and mechanical properties. Soft Matter 2006; 2:986-92. .

42. Kim A, Lakshman N, Petroll WM. Quantitative assessment of local collagen matrix remodeling in 3-D culture: the role of Rho kinase. Exp Cell Res 2006; 312:3683-92. [PMID: 16978606].

43. Grinnell F. Fibroblast-collagen matrix contraction: growth-factor signalling and mechanical loading. Trends Cell Biol 2000; 10:362-5. [PMID: 10932093].

44. Barocas VH, Moon AG, Tranquillo RT. The fibroblast-populated collagen microsphere assay of cell traction force–Part 2: Measurement of the cell traction parameter. J Biomech Eng 1995; 117:161-70. [PMID: 7666653].

45. Leung LY, Tian D, Brangwynne CP, Weitz DA, Tschumperlin DJ. A new microrheometric approach reveals individual and cooperative roles for TGF-beta1 and IL-1beta in fibroblast-mediated stiffening of collagen gels. FASEB J 2007; 21:2064-73. [PMID: 17341683].

46. Miron-Mendoza M, Lin X, Ma L, Ririe P, Petroll WM. Individual versus collective fibroblast spreading and migration: regulation by matrix composition in 3D culture. Exp Eye Res 2012; 99:36-44. [PMID: 22838023].

47. Hadjipanayi E, Mudera V, Brown RA. Guding cell migration in 3D: A collagen matrix with graded directional stiffness. Cell Motil Cytoskeleton 2009; 66:121-8. [PMID: 19170223].

48. Pang M, Zhuang S. Histone deacetylase: A potential therapeutic target for fibrotic disorders. J Pharmacol Exp Ther 2010; 335:266-72. [PMID: 20719940].

49. Adcock IM. HDAC inhibitors as anti-inflammatory agents. Br J Pharmacol 2007; 150:829-31. [PMID: 17325655].

50. Kitano A, Okada Y, Yamanka O, Shirai K, Mohan RR, Saika S. Therapeutic potential of trichostatin A to control

inflammatory and fibrogenic disorders of the ocular surface. Mol Vis 2010; 16:2964-73. [PMID: 21203344].

51. Vardouli L, Vasilaki E, Papadimitriou E, Kardassis D, Stournaras C. A novel mechanism of TGFbeta-induced actin reorganization mediated by Smad proteins and Rho GTPases. FEBS J 2008; 275:4074-87. [PMID: 18631173].

52. Hu B, Wu Z, Phan SH. Smad3 mediates transforming growth factor-beta-induced alpha-smooth muscle actin expression. Am J Respir Cell Mol Biol 2003; 29:397-404. [PMID: 12702545].

53. Harvey SA, Anderson SC, SundarRaj N. Downstream effects of ROCK signaling in cultured human corneal stromal cells: microarray analysis of gene expression. Invest Ophthalmol Vis Sci 2004; 45:2168-76. [PMID: 15223791].

54. Petroll WM, Ma L, Kim A, Ly L, Vishwanath M. Dynamic assessment of fibroblast mechanical activity during Rac-induced cell spreading in 3-D culture. J Cell Physiol 2008; 217:162-71. [PMID: 18452153].

55. Hubbert C, Guardiola A, Shao R, Kawaguchi Y, Ito A, Nixon A, Yoshida M, Wang XF, Yao TP. HDAC6 is a microtubule-associated deacetylase. Nature 2002; 417:455-8. [PMID: 12024216].

56. Catania A, Iavarone C, Carlomagno SM, Chiariello M. Selective transcription and cellular proliferation induced by PDGF require histone deacetylase activity. Biochem Biophys Res Commun 2006; 343:544-54. [PMID: 16554031].

57. Kiuchi N, Nakajima K, Ichiba M, Fukada T, Narimatsu M, Mizuno K, Hibi M, Hirano T. STAT3 is required for the gp130-mediated full activation of the c-myc gene. J Exp Med 1999; 189:63-73. [PMID: 9874564].

58. Konnikova L, Kotecki M, Kruger MM, Cochran BH. Knockdown of STAT3 expression by RNAi induces apoptosis in astrocytoma cells. BMC Cancer 2003; 3:23-[PMID: 13678425].

59. Funamoto M, Fujio Y, Kunisada K, Negoro S, Tone E, Osugi T, Hirota H, Izumi M, Yoshizaki K, Walsh K, Kishimoto T, Yamauchi-Takihara K. Signal transducer and activator of transcription 3 is required for glycoprotein 130-mediated induction of vascular endothelial growth factor in cardiac myocytes. J Biol Chem 2000; 275:10561-6. [PMID: 10744750].

60. Tran AD-A, Marmo TP, Salam AA, Che S, Finkelstein E, Kabarriti R, Xenias HS, Mazitschek R, Hubbert C, Kawaguchi Y, Sheetz MP, Yao T-P, Bulinski JC. HDAC6 deacetylation of tubulin modulates dynamics of cellular adhesions. J Cell Sci 2007; 120:1469-79. [PMID: 17389687].

61. Matsuyama A, Shimazu T, Sumida Y, Saito A, Yoshimatsu Y, Seigneurin-Berny D, Osada H, Komatsu Y, Nishino N, Khochbin S, Horinouchi S, Yoshida M. In vivo destabilization of dynamic microtubules by HDAC6-mediated deacetylation. EMBO J 2002; 21:6820-31. [PMID: 12486003].

62. Gao YS, Hubbert CC, Lu J, Lee YS, Lee JY, Yao TP. Histone deacetylase 6 regulates growth factor-induced actin remodeling and endocytosis. Mol Cell Biol 2007; 27:8637-47. [PMID: 17938201].

63. Kovacs JJ, Murphy PJ, Gaillard S, Zhao X, Wu JT, Nicchitta CV, Yoshida M, Toft DO, Pratt WB, Yao TP. HDAC6 regulates Hsp90 acetylation and chaperone-dependent activation of glucocorticoid receptor. Mol Cell 2005; 18:601-7. [PMID: 15916966].

64. Bali P, Pranpat M, Bradner J, Balasis M, Fiskus W, Guo F, Rocha K, Kumaraswamy S, Boyapalle S, Atadja P, Seto E, Bhalla K. Inhibition of histone deacetylase 6 acetylates and disrupts the chaperone function of heat shock protein 90: a novel basis for antileukemia activity of histone deacetylase inhibitors. J Biol Chem 2005; 280:26729-34. [PMID: 15937340].

65. Zhang Y, Kwon S, Yamaguchi T, Cubizolles F, Rousseaux S, Kneissel M, Cao C, Li N, Cheng HL, Chua K, Lombard D, Mizeracki A, Matthias G, Alt FW, Khochbin S, Matthias P. Mice lacking histone deacetylase 6 have hyperacetylated tubulin but are viable and develop normally. Mol Cell Biol 2008; 28:1688-701. [PMID: 18180281].

Articles are provided courtesy of Emory University and the Zhongshan Ophthalmic Center, Sun Yat-sen University, P.R. China. The print version of this article was created on 29 April 2015. This reflects all typographical corrections and errata to the article through that date. Details of any changes may be found in the online version of the article.